Ultrafast modulation of exciton-plasmon coupling in monolayer WS_2-Ag nanodisk hybrid system

Wei Du[1†], Jiaxin Zhao[1†], Weijie Zhao[1], Shunping Zhang[2], Hongxing Xu[2,3], Qihua Xiong[1,4,5]*

[1]*Division of Physics and Applied Physics, School of Physical and Mathematical Sciences, Nanyang Technological University, Singapore 637371*

[2]*School of Physics and Technology, Center for Nanoscience and Nanotechnology, and Key Laboratory of Artificial Micro- and Nano-structures of Ministry of Education, Wuhan University, 430072, Wuhan, China*

[3]*The Institute for Advanced Studies, Wuhan University, 430072, Wuhan, China*

[4]*MajuLab, International Joint Research Unit UMI 3654, CNRS, Université Côte d'Azur, Sorbonne Université, National University of Singapore, Nanyang Technological University, Singapore.*

[5]*NOVITAS, Nanoelectronics Center of Excellence, School of Electrical and Electronic Engineering, Nanyang Technological University, Singapore 639798*

[†]*These authors contributed equally to this work*

**To whom correspondence should be addressed. Email address: Qihua@ntu.edu.sg*

Abstract:

The rapid advances of nanotechnology and nanophotonics bring new approaches for manipulating light-matter interactions at the nanoscale, for example, by integrating plasmonic nanostructures with two-dimensional transition metal dichalcogenides (TMDs) to achieve strong exciton-plasmon interactions for applications in optical switches, sensing, and photovoltaic devices. Such TMD-plasmonic coupled system provides a highly unexplored territory towards understanding the exciton-plasmon interactions for ultrafast operations. Utilizing transient absorption pump-probe spectroscopy, here we report an ultrafast modulation of the exciton-plasmon coupling in a monolayer WS_2-Ag nanodisk hybrid system which displays Fano resonance at the steady-state regime. Specifically, the instant switch-off of the Fano resonance was observed upon the femtosecond pump excitation, characterized by the photo-induced absorption signal at the Fano resonance frequency. The fast recovery of the Fano resonance starts at the sub-100 femtosecond timescale as a result of the energy transfer from excitons of WS_2 to plasmons in Ag nanodisks. The slow recovery lasts for several tens of picoseconds, following the carrier relaxations in the subsystems. The ultrafast modulation of the exciton-plasmon coupling in the integrated TMD-plasmonic hybrid system will offer new opportunities for technologically relevant high-speed active plasmonic devices.

Keywords:

Plasmons, exciton, ultrafast, pump-probe spectroscopy, two-dimensional materials

TOC:

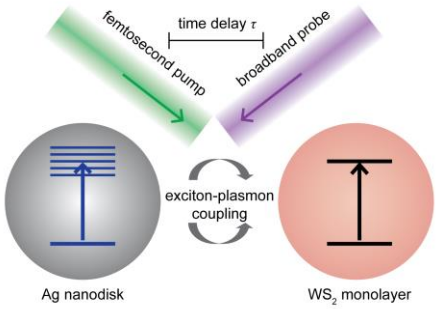

Introduction

Exciton-plasmon hybrid systems by coupling quantum emitters with plasmonic nanostructures have attracted intense research interest recently.[1–3] The understanding of such coupling provides knowledge for manipulating light-matter interactions involving surface plasmons towards augmented spatial or temporal performance in sub-wavelength nanophotonics, for instance, plasmon enhanced fluorescence,[4–7] plasmonic lasers,[8,9] and plasmonic switches.[10,11] Despite of the intrinsic heavy losses, plasmonic nanosystems are favoured for their highly confined electric field with a small modal volume, which usually leads to stronger coupling strength than that of dielectric based microcavities. Among the varieties of semiconducting materials, two-dimensional transition metal dichalcogenides (TMDs, in the form of MX_2, with M = Mo, W, etc. and X = S, Se, or Te) exhibit fascinating optical properties,[12–17] including tunable and layer thickness dependent band gaps, large dipole momentum, high exciton binding energy, strong spin-orbit coupling, and strong nonlinear response, offering an ideal platform for the study of exciton-plasmon interactions.

Depending on the energy exchange rate between the subsystems, different coupling regimes have been identified in the TMD-plasmonic hybrid systems, such as the weak coupling regime giving rise to the plasmon-enhanced luminescence,[4–7] the strong coupling regime featuring the Rabi splitting with the formation of two half-light half-matter polaritonic states,[18–23] and the intermediate coupling regime typically showing Fano-type interference together with photoluminescence enhancement.[24–27] It has also been demonstrated that the exciton-plasmon coupling in TMD-plasmonic hybrid system can be tuned actively to switch between different coupling regimes *via* electrostatic gating, which suggests the applications in active photonic devices.[28–30] In spite of the exciting progress, prior investigations were focused on the steady-state regime, leaving the dynamics of the TMD-plasmonic hybrid system largely unattended. Towards applications like ultrafast optical switches or photodetectors, it is remarkably important to understand the dynamical behavior of the hybrid system in the ultrafast timescale, for instance, how quickly the exciton-plasmon coupling can respond to an external ultrafast stimulus and whether it is charge transfer or energy transfer that dominates, following the instantaneous femtosecond response. In the concurrent limited reports involving time-resolved pump-probe experiments,[31–37]

those studies typically employed TMD-plasmonic hybrid samples with mismatched exciton and plasmon energy, resulting in mainly weak exciton-plasmon interactions. We therefore believe that the optical response of the TMD-plasmonic hybrid system to the ultrafast stimulus will largely depend on the initial coupling strength between excitons and plasmons in the steady-state, which will further alter the dynamics of the hybrid system in nontrivial ways.

Herein we have studied the exciton-plasmon coupling in the monolayer WS_2-Ag nanodisk hybrid system at both steady-state and ultrafast transient domain. With near resonant exciton-plasmon interaction, the hybrid system displays a pronounced Fano resonance feature in the steady-state optical spectra, corresponding to an intermediate exciton-plasmon coupling regime. The ultrafast modulation of the exciton-plasmon coupling in the WS_2-Ag hybrid structure was probed as a function of the pump-probe delay time τ via transient absorption spectroscopy. Following the femtosecond pump laser excitation, the instant decreasing of the exciton-plasmon coupling results in the photo-induced absorption signal at the Fano resonance frequency with two neighbouring bleaching signals. Furthermore, on a sub-100 femtosecond time scale we have visualized a quick recovery of the Fano resonance due to the energy transfer from excitons to plasmons, followed by a slow recovery on the picosecond timescale as a result of the intrinsic carrier relaxations in the subsystems. Our results are substantially different from previous observations reported in literature[31–37] with the similar TMD-plasmonic hybrid systems involving weak exciton-plasmon interactions, but are more similar to strongly coupled J-aggregated exciton-plasmon systems[38–42], indicating that exciton-plasmon coupling strength has a crucial influence on the ultrafast optical behavior of the hybrid system. The demonstrated ultrafast modulation of the Fano resonance also underpins the promising applications of TMD-plasmonic hybrid structures as high-frequency plasmonic devices such as ultrafast plasmonic switches or modulators.

Results and Discussion

Figure 1a illustrates the schematic diagram of the monolayer WS_2-Ag nanodisk hybrid structure studied in our experiments. The Ag nanodisks with a height of 40 nm, a spacing of 300 nm, and various diameters were fabricated on glass

substrates using electron beam lithography (Methods section). Figure 1b presents the typical SEM image of the Ag nanodisks with a 100 nm diameter. Figure 1c-d shows the optical images of a mechanically exfoliated WS_2 monolayer on polydimethylsiloxane (PDMS) and the corresponding hybrid sample (refer to the Supplementary Information Figure S1 for the PL spectra of WS_2 monolayer and the hybrid sample). The white dashed line in Fig. 1d highlights the boundary of the WS_2 monolayer specimen. In the presented sample (Fig. 1d), the Ag nanodisk diameter of each row increases from 70 nm to 150 nm with a step of 10 nm from top to bottom, leading to a systematic color change due to the red shift of the plasmon resonance. We note that it is not necessary to remove the PDMS film from the sample after transfer. From the calculated (FDTD Solutions, Lumerical, see Methods) electric field intensity distribution of the Ag nanodisk with (Fig. 1e) and without (Fig. 1f) the PDMS superstrate, we can clearly see that the existence of the PDMS superstrate actually enhances the electric field intensity at the top interface where the WS_2 monolayer locates and hence improves the exciton-plasmon coupling. Here the transition dipole moment of excitons in the WS_2 monolayer is oriented in-plane which mainly couples to the in-plane component of the plasmonic field (refer to the Supplementary Information Figure S2 for more details). The PDMS also serves as an extra protection layer to reduce unwanted oxidation of Ag exposed to ambient conditions.

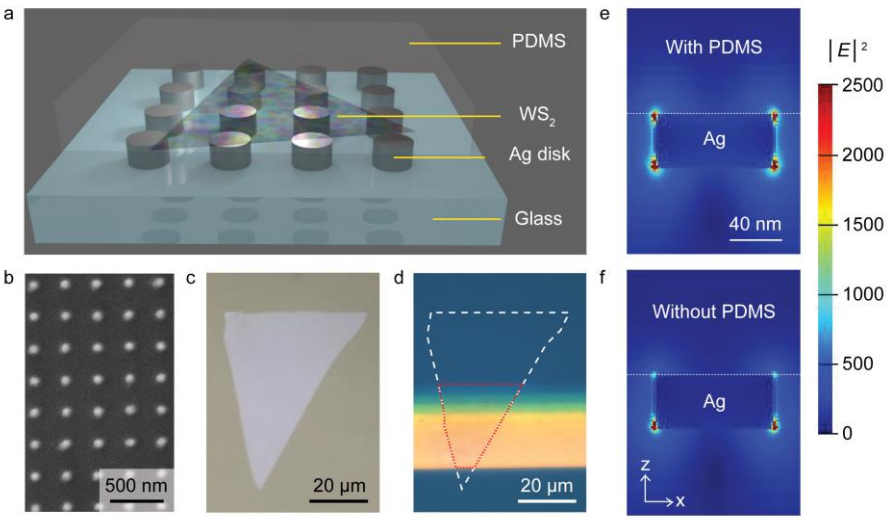

Figure 1. Monolayer WS_2-Ag nanodisk hybrid structure. a, Schematic of the monolayer WS_2-Ag nanodisk hybrid structure. **b,** SEM image of the Ag nanodisks with height of 40 nm, diameter of 100 nm, and spacing of 300 nm. **c,** Optical

micrograph of a monolayer WS_2 on PDMS. **d,** Optical micrograph of the hybrid sample with the monolayer WS_2 transferred onto the Ag nanodisks with varying disk diameters. The white dashed line indicates the boundary of the WS_2 monolayer and the red dotted line marks the region of the patterned Ag nanodisks covered by the WS_2 monolayer. **e, f** Calculated electric field intensity distribution of the Ag nanodisk on the glass substrate with (**e**) and without (**f**) the PDMS superstrate. The white dotted line indicates the position of the WS_2 monolayer.

To investigate the exciton-plasmon coupling in the WS_2-Ag nanodisk hybrid structure, we first conducted steady-state spectroscopy measurements in ambient conditions. Figure 2a shows the reflectivity spectra of bare Ag nanodisks recorded using an objective with a numerical aperture NA = 0.45 (corresponding to incidence and collection angles of ~0-27°). The angle dependent plasmonic lattice resonance modes[43–45] interact with the localized surface plasmon mode of the Ag nanodisks to form a single plasmon resonance peak (with a linewidth of ~300 meV, as shown in Fig. 2a). The plasmon resonance was tuned by adjusting the Ag nanodisk diameters and therefore we can control the detuning between the plasmon energy and the A exciton energy (~2.02 eV at room temperature[19,25]) of WS_2 monolayers. The corresponding reflectivity spectra of the WS_2-Ag hybrid structure, as shown in Fig. 2b, display a pronounced Fano resonance dip (FD) around the A exciton energy and two peaks on the left and right, defined as the low energy (LE) and high energy (HE) branches, respectively. Here, the two branches do not represent the two quantum states as the case in the strong coupling regime.[18–23] Instead, the observed features originate from the interference[46] between the exciton and plasmon, where the constructive and destructive interference results in the enhanced and reduced signal respectively, close to the A exciton energy. Such an interference effect is superimposed on the plasmon resonance response, generating the hybrid optical spectra. Hence we consider that our monolayer WS_2-Ag nanodisk hybrid system satisfies intermediate exciton-plasmon coupling regime and similar results have also been reported by other colleagues.[24–27] The experimental reflectivity spectra of the hybrid structure could be fitted using a previously developed Fano resonance model by considering two coupled oscillators in the classical system (Eq. 1)[47]:

$$a = \frac{(\omega_2^2 - \omega^2 + i\gamma_2\omega)}{(\omega_1^2 - \omega^2 + i\gamma_1\omega)(\omega_2^2 - \omega^2 + i\gamma_2\omega) - \nu_{12}^2} \quad (1)$$

Where a represents the amplitude of the Fano resonance (normalized to the plasmon resonance), ω_1 and ω_2 are the frequency of the plasmon and exciton, γ_1 and γ_2 are the damping rate of the plasmon and exciton, and ν_{12} describes the coupling strength between the two oscillators. The fitting results are shown in Fig. 2c, which well reproduces the experimental spectra in Fig. 2b. From the fitting, we could also extract the information of the uncoupled plamon and exciton resonances and their coupling strength (refer to the Supplementary Information Table S1 for more details).

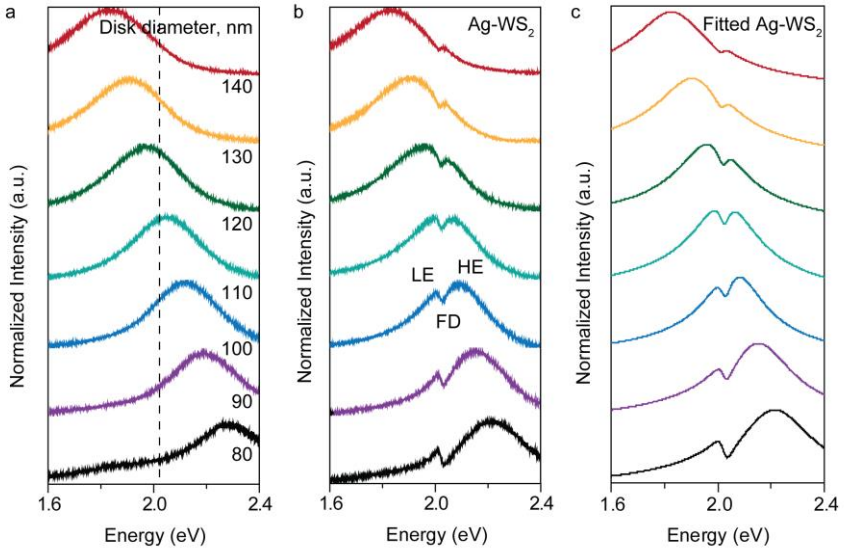

Figure 2. Exciton-plasmon coupling in the monolayer WS_2-Ag nanodisk hybrid system studied in the steady-state regime. a, Reflectivity spectra of bare Ag nanodisks (with PDMS superstrate) with disk diameters in the range of 80-140 nm. The black dashed line indicates the A exciton energy of the WS_2 monolayer. **b,** Reflectivity spectra of the monolayer WS_2-Ag nanodisk hybrid structure with the same nanodisk diameters as in panel **a**. **c,** Fitted optical spectra of the WS_2-Ag nanodisk hybrid structure based on experimental data presented in panel **b**.

The ultrafast dynamics of both uncoupled subsystems and the hybrid structure is further investigated at room temperature using pump-probe transient absorption

spectroscopy under near-resonant pumping at 598 nm. Detailed sample preparation and optical setup can be referred to the Methods section and Supplementary Information (Figure S3). Figure 3a-b plots the differential transmission mapping $\frac{\Delta T}{T}(\lambda,\tau)$ from the WS_2 monolayer and the bare Ag nanodisks, showing the photo-induced bleaching signals at the intrinsic exciton and plasmon resonance wavelength, respectively. Figure 3d-e provides the distinct time evolution of the $\frac{\Delta T}{T}(\lambda,\tau)$ signal for the WS_2 monolayer and the Ag nanodisks in two regimes: (i) -0.5 to 5 ps; (ii) -10 to 300 ps. We fitted the kinetics of both using multi-exponential decay functions (refer to Table S2 and Figure S4). Three lifetime values were extracted from the WS_2 monolayer: $t_{1,\,WS_2} = 170 \pm 50$ fs, $t_{2,\,WS_2} = 2.7 \pm 0.6$ ps and $t_{3,\,WS_2} = 68 \pm 12$ ps. Such a three-component dynamical process has been widely reported for TMDs in the literature,[48–51] although the physical origins of some processes are still under discussion. Different from bulk semiconductors, the strongly confined two-dimensional TMD materials exhibit room-temperature stable bound excitons with unique internal structure and many-body interactions, resulting in plentiful carrier dynamics ranging from fs to ps timescale. In our experiment, $t_{1,\,WS_2}$ is considered as the intrinsic radiative lifetime of the small-momentum 1s exciton which has been proven in the literature.[52] Here the ~100 fs radiative decay of 1s exciton at $K \approx 0$ is only possible with near-resonant pump excitation, which is 10 times faster than the typically reported ~1 ps lifetime of free electron-hole pairs under above-bandgap excitation. Besides the ultrafast radiative decay, the optically pumped excitons can also go through exciton-exciton or exciton-phonon scattering and turn into dark state. Hence $t_{2,\,WS_2}$ is resulting from non-radiative recombination via defects (trapped state) or Auger-type recombination. The $t_{3,\,WS_2}$ lasting till ~100 ps is then related to thermal effect, and corresponds to the cooling of the lattice. Two lifetime values were obtained for bare Ag nanodisks. The shorter one ($t_{1,\,Ag} = 1.07 \pm 0.05$ ps) mainly originates from the electron-phonon coupling (probably with a partial contribution from the electron-electron scattering), leading to heating of the lattice.[53] The longer one ($t_{2,\,Ag} = 145 \pm 71$ ps) corresponds to the energy transfer from the lattice to the environment, *i.e.*, cooling of the lattice.[53] The plasmon lifetime of the Ag nanodisk,

which is expected to be less than 10 fs,[53] could not be captured in our experiments due to the time resolution of our setup. The observed temporal oscillations are related to the acoustic breathing modes of the Ag nanodisks.[54–57] With the fast Fourier transform (FFT) analysis (see Figure S5), we extracted two main oscillation frequencies of 0.02 THz (corresponding to phonon energy of 82.7 μeV) and 0.0125 THz (corresponding to phonon energy of 51.7 μeV) which may be attributed to the different modes due to the asymmetric coupling to the glass substrate and PDMS superstrate.

The measured $\frac{\Delta T}{T}(\lambda,\tau)$ for the WS_2-Ag hybrid structure (Fig. 3c), however, exhibits new features that are apparently not the simple sum of the two uncoupled subsystems. Instead, we observed a photo-induced absorption signal (negative $\frac{\Delta T}{T}$) at the FD accompanied by two photo-induced bleaching signals at the HE and LE branches. The negative $\frac{\Delta T}{T}$ corresponds to a decreased transmission in the FD, which essentially reveals a modulated Fano resonance induced by the femtosecond pump laser. Figure 3f plots the time evolution of the $\frac{\Delta T}{T}$ signal for HE, FD and LE respectively in two regimes: (i) -0.5 to 1.5 ps; (ii) -10 to 300 ps (ii). With a detailed analysis (refer to the lifetime fitting in Table S2 and Figure S4), we could also deduce a three-component dynamical process for the hybrid structure. First of all, we visualize an ultrafast component within ~100 fs after the pump pulse, characterized by an increase of $\frac{\Delta T}{T}$ signal at FD (with fitted lifetime value $t_{1,\,\mathrm{FD}} = 24 \pm 4$ fs) along with a decrease of $\frac{\Delta T}{T}$ signal at HE (with fitted lifetime value $t_{1,\,\mathrm{HE}} = 34 \pm 3$ fs). Such an ultrafast response (~5 times faster than $t_{1,\,WS_2}$ and more than 30 times faster than $t_{1,\,Ag}$) may indicate the energy or charge transfer between the WS_2 monolayer and the Ag nanodisks. The subsequent two components are on the timescale of 1-10 ps and 10-100 ps, respectively, and are similar to the intrinsic dynamical behavior of the WS_2 monolayer and the bare Ag nanodisks on the same timescale. Last but not the least, temporal oscillations due to the acoustic breathing modes were also observed in the hybrid structure, which are similar to that of the bare Ag nanodisks.[54–57]

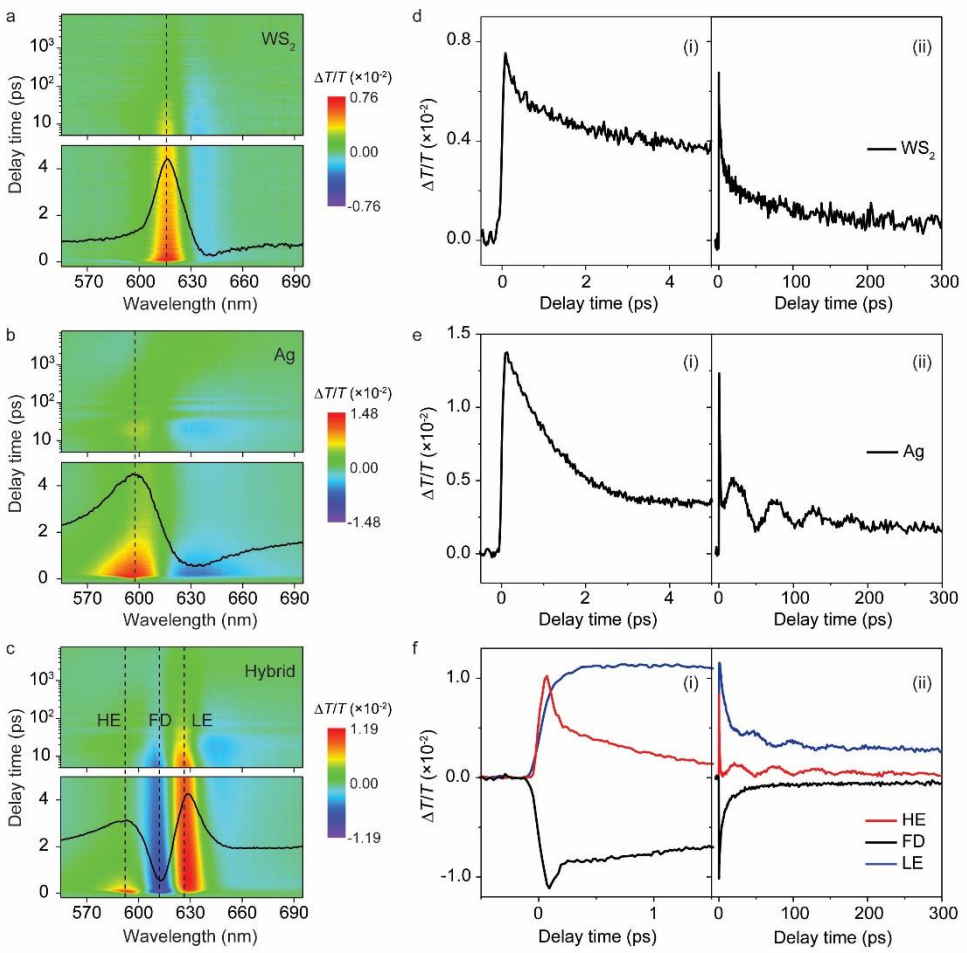

Figure 3. Ultrafast dynamics of the exciton-plasmon coupling in the WS_2-Ag hybrid structure in comparison to the uncoupled subsystems. a-c, $\frac{\Delta T}{T}(\lambda,\tau)$ for the WS_2 monolayer (**a**), Ag nanodisks (**b**), and WS_2-Ag hybrid structure (**c**) with a disk diameter of ~110 nm. The pump has a wavelength of 598 nm and fluence of 19.2 μJ/cm^2. The solid black curves in three plots are the representative spectra with a horizontal cut at a pump-probe delay time of 250 fs. **d, e** Time evolution of the $\frac{\Delta T}{T}$ signal for the WS_2 monolayer (**d**) and Ag nanodisks (**e**) with pump-probe delay time of -0.5 to 5 ps (i) and -10 to 300 ps (ii). **f,** Time evolution of the $\frac{\Delta T}{T}$ signal for HE, FD and LE in the WS_2-Ag hybrid structure with a pump-probe delay time of -0.5 to 1.5 ps (i) and -10 to 300 ps (ii).The probe wavelengths for WS_2, Ag, HE, FD and LE are indicated respectively by the vertical dashed lines in **a-c**.

The ultrafast optical response and dynamics of the WS_2-Ag hybrid system can be understood using a simple physical model shown in Figure 4 which describes the modulation of the exciton-plasmon coupling (or Fano resonance) as a function of the pump-probe delay time. Before the pump arrives (at $\tau < 0$, Fig. 4a), the hybrid system is in the intermediate exciton-plasmon coupling regime, showing Fano-type interference with electromagnetically induced transmission[58] at FD (around the A exciton energy, refer to the steady-state measurement in Figure S1). With the femtosecond pump laser excitation (at $\tau = 0$, Fig. 4b), electrons were injected into the excited state at the WS_2 monolayer. Consequently, the ground state absorption of the WS_2 monolayer will decrease, leading to reduced effective oscillator strength f_2 with increased damping rate γ_2 for the excitonic resonance. Based on eq. 1, the increased γ_2 will modify the lineshape of the Fano resonance and hence we could calculate the $\frac{\Delta T}{T}$ signal for the WS_2–Ag hybrid structure induced by the femtosecond pump laser (refer to the Supplementary Information Figure S6 and Table S3 for more details). The calculated result matches well with our experimental data qualitatively with negative $\frac{\Delta T}{T}$ at the FD and positive $\frac{\Delta T}{T}$ at the HE and LE branches, indicating the reduced Fano resonance with the pump pulse excitation. The differences in the relative intensities of the three features (HE, FD and LE) between experiment and calculation may come from pump induced electron injection and plasmon excitation in the Ag nanodisk, which could also contribute to the transient signal of the hybrid structure although it should not be a dominating effect considering the large amount of free electrons in the Ag nanodisk (see Figure S7 and Table S4 in the Supplementary Information). In addition, it has also been well documented that the changes in the exciton oscillator strength f_2 will affect the strength of the exciton-plasmon coupling ν_{12} as $\nu_{12} \propto \sqrt{f_2}$.[59,60] Thus a more complex calculation can be made by involving related changes in both γ_2 and ν_{12} by assuming $\Delta\nu_{12} \propto \sqrt{\frac{1}{\Delta\gamma_2}}$ (refer to the Supplementary Information Figure S8 and Table S5).

After the pump pulse, the decay of surface plasmons is too fast to be probed as evidenced by the transient spectrum of bare Ag nanodisks. However, the radiative

decay of excitons in the WS_2 monolayer could transfer their energy to surface plasmons in the Ag nanodisks and hence initiate the exciton-plasmon energy exchange on a sub-100 fs timescale before relaxation in other pathways (Fig. 4c). Accordingly, the constructive and destructive interference between excitons and surface plasmons will lead to a quick recovery of the Fano resonance.[27] In our experiment, the extracted lifetime value for this exciton-plasmon energy exchange process is 29 ± 5 fs (by averaging the fitted lifetime values for FD and HE branches) that is 5 times shorter than the intrinsic radiative decay lifetime ($t_{1,\,WS_2} = 170 \pm 50$ fs) of the exciton in the WS_2 monolayer benefiting from the plasmonic field enhancement effect.[61] In the end, with longer pump-probe delay times (τ > 100 fs), the excited-state carriers in both WS_2 monolayer and Ag nanodisks further relax via carrier-carrier scattering or interaction with phonons. The time-dependent decreasing of the excited-state populations could induce a further slow recovery of the Fano resonance until all the excited carriers relax to the ground state.

Besides the exchange of energy, we have also considered the possibility of plasmon-induced hot electron transfer[31,33,37,62–66] from the Ag nanodisks to the WS_2 monolayer which has been widely reported by other groups at the metal-TMD interfaces and is expected to happen at a similar timescale. However, such a directional charge transfer should result in further increased excited-state populations in the WS_2 monolayer, leading to further decreased exciton-plasmon coupling, which is in stark contrast to the quick recovery of the Fano resonance observed by us. In addition, the hot electron transfer picture can not explain the ultrafast optical response of our WS_2-Ag hybrid system which is not a simple superimposition of the transient signals from the two sub-systems. Based on the above discussions, we believe that hot electron transfer is not a dominating process in our results.

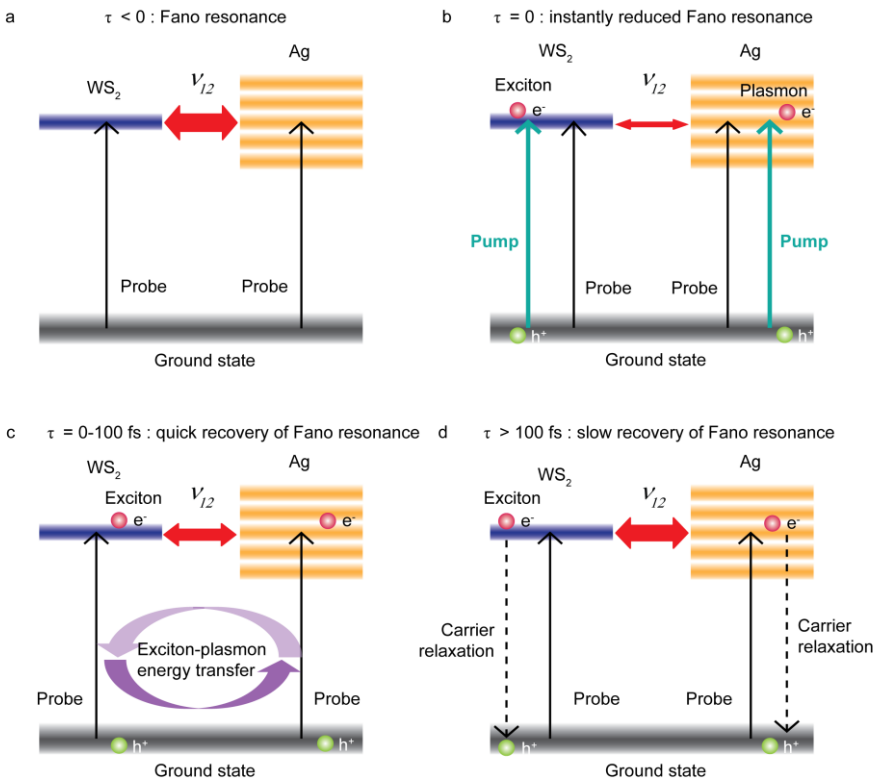

Figure 4. Schematic illustration of the ultrafast modulation of exciton-plasmon coupling in the WS_2-Ag hybrid structure at different pump-probe delay time. a, At τ < 0, the exciton-plasmon coupling in the hybrid system shows Fano-type interference. **b,** At τ = 0, the femtosecond pump laser induces decreased exciton-plasmon coupling with reduced Fano feature. **c,** With τ = 0-100 fs, the energy transfer between excitons and plasmons leads to quickly increased exciton-plasmon coupling and fast recovery of the Fano resonance. **d,** With τ > 100 fs, the intrinsic carrier relaxations in the WS_2 monolayer and Ag nanodisks result in further increased exciton-plasmon coupling and slow recovery of the Fano resonance. The different widths of the red double-arrows in **a-d** schematically illustrate the changes in the exciton-plasmon coupling strength v_{12}.

The ultrafast modulation of the exciton-plasmon coupling can be further controlled by the pump fluence. Figure 5a-b shows the measured $\frac{\Delta T}{T}(\lambda,\tau)$ for the WS_2-Ag hybrid structure with the pump fluence of 2.4 and 76.8 μJ/cm^2, respectively (See Figure S9 for more data with intermediate pump fluences). It is interesting to

note that at the lower pump fluence the FD and LE branches have higher signals than the HE branch while the opposite happens at the higher pump fluence. Such a phenomenon is due to the different pump fluence dependency of each branch. As shown in Fig. 5c, we observed that the pump fluence modulates the signal of the HE branch linearly with the slope of 4.2×10^{-4}. By contrast, the signals at the FD and LE branches show a clear saturation behavior vs. pump fluence. These pump fluence modulation behaviors may be better understood from the bare Ag nanodisks and the pristine WS_2 monolayer cases (Fig. 5d). Similar to the HE branch case, the $\frac{\Delta T}{T}$ signal of the Ag nanodisks shows a linear dependence vs. pump fluence with a slope of 5.1×10^{-4}, indicating that the HE branch in the hybrid structure mainly represents the feature of the plasmon resonance. However, the $\frac{\Delta T}{T}$ signal of the WS_2 monolayer also shows a linear behavior (with the slope of 1.6×10^{-3}) in the studied pump fluence range, which is different from the saturation behavior of the FD (or LE) branch. The saturation observed in the FD (or LE) branch may point to an earlier saturation of the WS_2 at lower pump fluences in the WS_2-Ag hybrid structure compared to the case in the bare WS_2 monolayer, reflecting the plasmonic modulation effect on the WS_2 monolayer. Such a result essentially ensures the efficient modulation of these TMD-plasmonic hybrid devices at relatively low pump fluences.

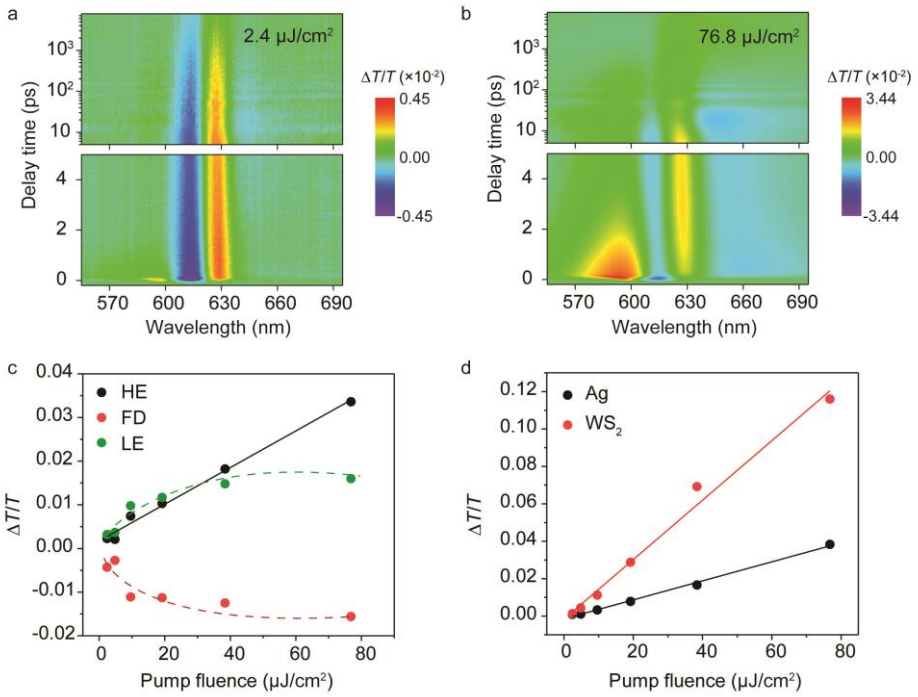

Figure 5. Pump fluence dependence of the ultrafast modulation of exciton-plasmon coupling. a, b $\frac{\Delta T}{T}(\lambda,\tau)$ for the WS_2-Ag hybrid structure using pump wavelength of 598 nm with pump fluences of 2.4 μJ/cm^2 and 76.8 μJ/cm^2. **c**, The plot of $\frac{\Delta T}{T}$ at HE, FD and LE for the WS_2-Ag hybrid structure as a function of the pump fluences. **d,** The plot of $\frac{\Delta T}{T}$ for the bare Ag nanodisks and WS_2 monolayer as a function of the pump fluences. The sold lines in panels **c** and **d** are linear fits to the data. The dashed lines in panel **c** serve as a guide to the eye.

Conclusion

In summary, we have studied both the steady-state and the ultrafast optical response of the monolayer WS_2-Ag hybrid system. The steady-state spectra show an intermediate coupling between excitons of WS_2 monolayer and plasmons of the Ag nanodisks with the Fano resonance line-shape. Via transient absorption study, we visualized the ultrafast modulation of the exciton-plasmon coupling in the hybrid system, showing instant switch-off and further recovery of the Fano resonance on the timescale of sub-100 fs, induced by the energy transfer between excitons and plasmons. Although the ultrafast modulation of the exciton-plasmon coupling to switch between different coupling regimes by femtosecond lasers have been previously investigated in molecular aggregate and plasmonic coupled system,[39,41,42] our results demonstrate the similar principle applied to the TMD-plasmonic hybrid system where an atomic layer of material could also display pronounced modulations due to the fascinating excitonic properties of TMDs. Our results highlight the promising future of ultrafast plasmonic switches or sensors, by integrating two-dimensional TMDs with plasmonic nanostructures.

Methods

Sample Preparation. We fabricated the Ag nanodisks with different diameters using electron beam lithography. Positive resist (950 PMMA A4, Microchem, USA) was spin-coated (4000 rpm, 60 s) on the pre-cleaned glass substrate and baked at 180 ℃ for 3 mins, resulting in a PMMA film with thickness of ~200 nm. After PMMA baking, Espacer 300Z (Showa Denko, Singapore) was spin coated (1500 rpm, 60 s) on top of PMMA to reduce the charging induced by non-conductive substrate during the electron beam exposure. We did the patterning using a JEOL 7001F scanning electron microscope equipped with NPGS (nanometer pattern generation system) software. The exposed sample was cleaned with DI water first to wash away the Espacer and then immersed in the developer (MIBK:IPA = 1:3) for 90 s followed by IPA washing and N_2 dry. After development, we did the metal deposition (40 nm Ag with 1 nm Cr adhesion layer) using a thermal evaporator (Elite Engineering, Singapore). The lift-off was done in acetone and ended with IPA rinsing and N_2 dry of the sample. The WS_2 monolayer was mechanically exfoliated onto a transparent PDMS film first and then identified via the fluorescence emission. In the end, we transferred the selected WS_2 monolayer on top of the pre-fabricated Ag nanodisks using a transfer stage to finish the preparation of the hybrid structure.

Optical Measurement. (1) Reflectivity spectra (shown in Figure 2) were collected using the Horiba-JY HR800 spectrometer equipped with a white-light source. With a 50× objective and a small aperture size of 100 μm, we are able to measure sample size down to 2 μm which facilitates the detuning experiment. (2) For the transmission measurement (data in Fig. S1c), we used the Craic 20 microspectrophotometer with which sample size of ~10 μm is needed. (3) Time-resolved pump-probe measurement was conducted utilizing a femtosecond transient absorption spectrometer (HELIOS, Ultrafast Systems). The femtosecond laser source with 800 nm central wavelength, 1 kHz repetition rate and ~100 fs pulse duration was splitted into two beams. The first beam was used to pump the optical parametric amplifier (TOPAS Prime) after which pump beam with tunable wavelength in the range of 260−2000 nm can be obtained. The second beam was focused onto a sapphire crystal to generate the probe beam (with wavelength range of 400 to 800 nm). The probe beam is perpendicular to the sample surface while the pump beam has an angle of ~45 degree with respective to the sample surface. Such a configuration allows transient absorption measurement

under resonant excitation condition. Both pump and probe beams focused on the same position (i.e., the position where we put the sample) with the delay time controlled by a motorized mechanical delay stage. The focused pump beam has a diameter of ~100 μm and the focused probe beam has a diameter of ~50 μm. Large-area hybrid sample (refer to Figure S1) was prepared for the transient absorption measurement using the same fabrication procedures described above.

Simulation. We calculated the electric field intensity distribution of the Ag nanodisk with (Fig. 1e) and without (Fig. 1f) the PDMS superstrate with the finite-difference time-domain (FDTD) method using "Lumerical FDTD Solutions" software. The Ag nanodisk has a diameter of 100 nm, height of 40 nm and spacing of 300 nm with the dielectric function of Ag taking from literature.[67] The WS_2 monolayer was modelled as a flat film with thickness of 1 nm and its dielectric function was taken from previous report.[68] The refractive index for the glass substrate, PDMS superstrate and air is respectively 1.5, 1.4 and 1.0.

ASSOCIATED CONTENT

Supporting Information

The Supporting Information is available free of charge on the ACS Publications website.

PL spectra of the WS_2 monolayer on flat glass substrate and on Ag nanodisks; FDTD simulation; Fano resonance fitting; Large-area WS_2-Ag hybrid sample; Lifetime fitting for both uncoupled subsystems and the hybrid system; Temporal oscillations due to acoustic phonon modes; Modelling of the $\frac{\Delta T}{T}$ signal for the WS_2–Ag hybrid structure with the pump pulse; Pump fluence dependence

AUTHOR INFORMATION

Corresponding Author

*Email address: Qihua@ntu.edu.sg

Author Contributions

W.D. and Q.H.X. conceived the idea and designed the research; W.D. fabricated all the samples; W.D. and J.X.Z performed the optical measurement. W.D., J.X.Z, W.J.Z and Q.H.X. analysed the data; W.D. and Q.H.X. wrote the manuscript. All authors discussed and commented on the manuscript.

Notes

The authors declare no competing financial interest.

Acknowledgement

Q.X. gratefully acknowledges the support from the Singapore National Research Foundation through the NRF-ANR grant (NRF2017-NRF-ANR005 2D-CHIRAL), and the Singapore Ministry of Education via AcRF Tier 3 grant (MOE2018-T3-1-002) and AcRF Tier 2 grant (MOE2017-T2-1-040).

References

(1) Hugall, J. T.; Singh, A.; Van Hulst, N. F. Plasmonic Cavity Coupling. *ACS Photonics* **2018**, *5*, 43–53.

(2) Vasa, P.; Lienau, C. Strong Light−Matter Interaction in Quantum Emitter/Metal Hybrid Nanostructures. *ACS Photonics* **2018**, *5*, 2–23.

(3) Cao, E.; Lin, W.; Sun, M.; Liang, W.; Song, Y. Exciton-Plasmon Coupling Interactions: From Principle to Applications. *Nanophotonics* **2018**, *7*, 145–167.

(4) Najmaei, S.; Mlayah, A.; Arbouet, A.; Girard, C.; Leotin, J.; Lou, J. Plasmonic Pumping of Excitonic Photoluminescence in Hybrid MoS_2-Au Nanostructures. *ACS Nano* **2014**, *8*, 12682–12689.

(5) Butun, S.; Tongay, S.; Aydin, K. Enhanced Light Emission from Large-Area Monolayer MoS_2 Using Plasmonic Nanodisc Arrays. *Nano Lett.* **2015**, *15*, 2700–2704.

(6) Wang, Z.; Dong, Z.; Gu, Y.; Chang, Y.; Zhang, L.; Li, L.; Zhao, W.; Eda, G.; Zhang, W.; Grinblat, G.; *et al.* Giant Photoluminescence Enhancement in Tungsten-Diselenide–Gold Plasmonic Hybrid Structures. *Nat. Commun.* **2016**, *7*, 11283.

(7) Hao, Q.; Pang, J.; Zhang, Y.; Wang, J.; Ma, L.; Schmidt, O. G. Boosting the Photoluminescence of Monolayer MoS_2 on High-Density Nanodimer Arrays with Sub-10 nm Gap. *Adv. Opt. Mater.* **2018**, *6*, 1700984.

(8) Berini, P.; De Leon, I. Surface Plasmon-Polariton Amplifiers and Lasers. *Nat. Photonics* **2012**, *6*, 16–24.

(9) Zhang, Q.; Li, G.; Liu, X.; Qian, F.; Li, Y.; Sum, T. C.; Lieber, C. M.; Xiong, Q. A Room Temperature Low-Threshold Ultraviolet Plasmonic Nanolaser. *Nat. Commun.* **2014**, *5*, 4953.

(10) Zheng, Y. B.; Kiraly, B.; Cheunkar, S.; Huang, T. J.; Weiss, P. S. Incident-Angle-Modulated Molecular Plasmonic Switches: A Case of Weak Exciton-Plasmon Coupling. *Nano Lett.* **2011**, *11*, 2061–2065.

(11) Pala, R. A.; Shimizu, K. T.; Melosh, N. A.; Brongersma, M. L. A Nonvolatile Plasmonic Switch Employing Photochromic Molecules. *Nano Lett.* **2008**, *8*, 1506–1510.

(12) Duan, X.; Wang, C.; Pan, A.; Yu, R.; Duan, X. Two-Dimensional Transition Metal Dichalcogenides as Atomically Thin Semiconductors: Opportunities and Challenges. *Chem. Soc. Rev.* **2015**, *44*, 8859–8876.

(13) Mak, K. F.; Shan, J. Photonics and Optoelectronics of 2D Semiconductor Transition Metal Dichalcogenides. *Nat. Photonics* **2016**, *10*, 216–226.

(14) Choi, W.; Choudhary, N.; Han, G. H.; Park, J.; Akinwande, D.; Lee, Y. H. Recent Development of Two-Dimensional Transition Metal Dichalcogenides and Their Applications. *Mater. Today* **2017**, *20*, 116–130.

(15) Berkelbach, T. C.; Reichman, D. R. Optical and Excitonic Properties of Atomically Thin Transition-Metal Dichalcogenides. *Annu. Rev. Condens. Matter Phys.* **2018**, *9*, 379–396.

(16) Xu, W.; Liu, W.; Schmidt, J. F.; Zhao, W.; Lu, X.; Raab, T.; Diederichs, C.; Gao, W.; Seletskiy, D. V.; Xiong, Q. Correlated Fluorescence Blinking in Two-Dimensional Semiconductor Heterostructures. *Nature* **2017**, *541*, 62–67.

(17) Jiang, C.; Xu, W.; Rasmita, A.; Huang, Z.; Li, K.; Xiong, Q.; Gao, W. Microsecond Dark-Exciton Valley Polarization Memory in Two-Dimensional Heterostructures. *Nat. Commun.* **2018**, *9*, 753.

(18) Liu, W.; Lee, B.; Naylor, C. H.; Ee, H.; Park, J.; Johnson, A. T. C.; Agarwal, R. Strong Exciton−Plasmon Coupling in MoS_2 Coupled with Plasmonic Lattice. *Nano Lett.* **2016**, *16*, 1262–1269.

(19) Wang, S.; Li, S.; Chervy, T.; Shalabney, A.; Azzini, S.; Orgiu, E.; Hutchison, J. A.; Genet, C.; Samorì, P.; Ebbesen, T. W. Coherent Coupling of WS_2 Monolayers with Metallic Photonic Nanostructures at Room Temperature. *Nano Lett.* **2016**, *16*, 4368–4374.

(20) Kleemann, M.; Chikkaraddy, R.; Alexeev, E. M.; Kos, D.; Carnegie, C.; Deacon, W.; De Pury, A. C.; Große, C.; De Nijs, B.; Mertens, J.; *et al.* Strong-

Coupling of WSe_2 in Ultra-Compact Plasmonic Nanocavities at Room Temperature. *Nat. Commun.* **2017**, *8*, 1296.

(21) Stührenberg, M.; Munkhbat, B.; Baranov, D. G.; Cuadra, J.; Yankovich, A. B.; Antosiewicz, T. J.; Olsson, E.; Shegai, T. Strong Light-Matter Coupling between Plasmons in Individual Gold Bi-Pyramids and Excitons in Mono- and Multilayer WSe_2. *Nano Lett.* **2018**, *18*, 5938–5945.

(22) Han, X.; Wang, K.; Xing, X.; Wang, M.; Lu, P. Rabi Splitting in a Plasmonic Nanocavity Coupled to a WS_2 Monolayer at Room Temperature. *ACS Photonics* **2018**, *5*, 3970–3976.

(23) Zheng, D.; Zhang, S.; Deng, Q.; Kang, M.; Nordlander, P.; Xu, H. Manipulating Coherent Plasmon-Exciton Interaction in a Single Silver Nanorod on Monolayer WSe_2. *Nano Lett.* **2017**, *17*, 3809–3814.

(24) Sun, J.; Hu, H.; Zheng, D.; Zhang, D.; Deng, Q.; Zhang, S.; Xu, H. Light-Emitting Plexciton: Exploiting Plasmon-Exciton Interaction in the Intermediate Coupling Regime. *ACS Nano* **2018**, *12*, 10393–10402.

(25) Wang, M.; Krasnok, A.; Zhang, T.; Scarabelli, L.; Liu, H.; Wu, Z.; Liz-marzán, L. M.; Terrones, M.; Alù, A.; Zheng, Y. Tunable Fano Resonance and Plasmon–Exciton Coupling in Single Au Nanotriangles on Monolayer WS_2 at Room Temperature. *Adv. Mater.* **2018**, *30*, 1705779.

(26) Abid, I.; Chen, W.; Yuan, J.; Bohloul, A.; Najmaei, S.; Avendano, C.; Pechou, R.; Mlayah, A.; Lou, J. Temperature-Dependent Plasmon−Exciton Interactions in Hybrid Au/$MoSe_2$ Nanostructures. *ACS Photonics* **2017**, *4*, 1653–1660.

(27) Lee, B.; Park, J.; Han, G. H.; Ee, H.; Naylor, C. H.; Liu, W.; Johnson, A. T. C.; Agarwal, R. Fano Resonance and Spectrally Modified Photoluminescence Enhancement in Monolayer MoS_2 Integrated with Plasmonic Nanoantenna Array. *Nano Lett.* **2015**, *15*, 3646–3653.

(28) Wen, J.; Wang, H.; Wang, W.; Deng, Z.; Zhuang, C.; Zhang, Y.; Liu, F.; She, J.; Chen, J.; Chen, H.; *et al.* Room-Temperature Strong Light-Matter Interaction with Active Control in Single Plasmonic Nanorod Coupled with Two-Dimensional Atomic Crystals. *Nano Lett.* **2017**, *17*, 4689–4697.

(29) Lee, B.; Liu, W.; Naylor, C. H.; Park, J.; Malek, S. C.; Berger, J. S.; Johnson, A. T. C.; Agarwal, R. Electrical Tuning of Exciton−Plasmon Polariton Coupling in Monolayer MoS_2 Integrated with Plasmonic Nanoantenna Lattice. *Nano Lett.* **2017**, *17*, 4541–4547.

(30) Chakraborty, B.; Gu, J.; Sun, Z.; Khatoniar, M.; Bushati, R.; Boehmke, A. L.; Koots, R.; Menon, V. M. Control of Strong Light-Matter Interaction in Monolayer WS_2 through Electric Field Gating. *Nano Lett.* **2018**, *18*, 6455–6460.

(31) Yu, Y.; Ji, Z.; Zu, S.; Du, B.; Kang, Y.; Li, Z.; Zhou, Z.; Shi, K.; Fang, Z. Ultrafast Plasmonic Hot Electron Transfer in Au Nanoantenna/MoS_2 Heterostructures. *Adv. Funct. Mater.* **2016**, *26*, 6394–6401.

(32) Kang, Y.; Li, B.; Fang, Z. Radiative Energy Transfer from MoS_2 Excitons to Surface Plasmons. *J. Opt.* **2017**, *19*, 124009.

(33) Shan, H.; Yu, Y.; Wang, X.; Luo, Y.; Zu, S.; Du, B.; Han, T.; Li, B.; Li, Y.; Wu, J.; *et al.* Direct Observation of Ultrafast Plasmonic Hot Electron Transfer

in the Strong Coupling Regime. *Light Sci. Appl.* **2019**, *8*, 9.

(34) Boulesbaa, A.; Babicheva, V. E.; Wang, K.; Kravchenko, I. I.; Lin, M. W.; Mahjouri-Samani, M.; Jacobs, C. B.; Puretzky, A. A.; Xiao, K.; Ivanov, I.; *et al.* Ultrafast Dynamics of Metal Plasmons Induced by 2D Semiconductor Excitons in Hybrid Nanostructure Arrays. *ACS Photonics* **2016**, *3*, 2389–2395.

(35) Lin, W.; Shi, Y.; Yang, X.; Li, J.; Cao, E.; Xu, X.; Pullerits, T.; Liang, W.; Sun, M. Physical Mechanism on Exciton-Plasmon Coupling Revealed by Femtosecond Pump-Probe Transient Absorption Spectroscopy. *Mater. Today Phys.* **2017**, *3*, 33–40.

(36) Xu, X.; Shi, Y.; Liu, X.; Sun, M. Femtosecond Dynamics of Monolayer MoS_2-Ag Nanoparticles Hybrid Probed at 532 nm. *Chem. Phys. Lett.* **2018**, *692*, 208–213.

(37) Wen, X.; Xu, W.; Zhao, W.; Khurgin, J. B.; Xiong, Q. Plasmonic Hot Carriers-Controlled Second Harmonic Generation in WSe_2 Bilayers. *Nano Lett.* **2018**, *18*, 1686–1692.

(38) Dintinger, J.; Robel, I.; Kamat, P. V; Genet, C.; Ebbesen, T. W. Terahertz All-Optical Molecule-Plasmon Modulation. *Adv. Mater.* **2006**, *18*, 1645–1648.

(39) Vasa, P.; Pomraenke, R.; Cirmi, G.; De Re, E.; Wang, W.; Schwieger, S.; Leipold, D.; Runge, E.; Cerullo, G.; Lienau, C. Ultrafast Manipulation of Strong Coupling in Metal-Molecular Aggregate Hybrid Nanostructures. *ACS Nano* **2010**, *4*, 7559–7565.

(40) Vasa, P.; Wang, W.; Pomraenke, R.; Lammers, M.; Maiuri, M.; Manzoni, C.; Cerullo, G.; Lienau, C. Real-Time Observation of Ultrafast Rabi Oscillations between Excitons and Plasmons in Metal Nanostructures with J-Aggregates. *Nat. Photonics* **2013**, *7*, 128–132.

(41) Fofang, N. T.; Grady, N. K.; Fan, Z.; Govorov, A. O.; Halas, N. J. Plexciton Dynamics: Exciton-Plasmon Coupling in a J-Aggregate-Au Nanoshell Complex Provides a Mechanism for Nonlinearity. *Nano Lett.* **2011**, *11*, 1556–1560.

(42) Nan, F.; Zhang, Y. F.; Li, X.; Zhang, X. T.; Li, H.; Zhang, X.; Jiang, R.; Wang, J.; Zhang, W.; Zhou, L.; *et al.* Unusual and Tunable One-Photon Nonlinearity in Gold-Dye Plexcitonic Fano Systems. *Nano Lett.* **2015**, *15*, 2705–2710.

(43) Wang, W.; Ramezani, M.; Väkeväinen, A. I.; Törmä, P.; Rivas, J. G.; Odom, T. W. The Rich Photonic World of Plasmonic Nanoparticle Arrays. *Mater. Today* **2018**, *21*, 303–314.

(44) Kravets, V. G.; Kabashin, A. V.; Barnes, W. L.; Grigorenko, A. N. Plasmonic Surface Lattice Resonances: A Review of Properties and Applications. *Chem. Rev.* **2018**, *118*, 5912–5951.

(45) Rajeeva, B. B.; Lin, L.; Zheng, Y. Design and Applications of Lattice Plasmon Resonances. *Nano Res.* **2018**, *11*, 4423–4440.

(46) Vasa, P.; Pomraenke, R.; Schwieger, S.; Mazur, Y. I.; Kunets, V.; Srinivasan, P.; Johnson, E.; Kihm, J. E.; Kim, D. S.; Runge, E.; *et al.* Coherent Exciton–Surface-Plasmon-Polariton Interaction in Hybrid Metal-Semiconductor Nanostructures. *Phys. Rev. Lett.* **2008**, *101*, 116801.

(47) Joe, Y. S.; Satanin, A. M.; Kim, C. S. Classical Anlogy of Fano Resonances. *Phys. Scr.* **2006**, *74*, 259–266.

(48) Sie, E. J.; Steinhoff, A.; Gies, C.; Lui, C. H.; Ma, Q.; Rösner, M.; Schönhoff, G.; Jahnke, F.; Wehling, T. O.; Lee, Y. H.; *et al.* Observation of Exciton Redshift-Blueshift Crossover in Monolayer WS_2. *Nano Lett.* **2017**, *17*, 4210–4216.

(49) Ruppert, C.; Chernikov, A.; Hill, H. M.; Rigosi, A. F.; Heinz, T. F. The Role of Electronic and Phononic Excitation in the Optical Response of Monolayer WS_2 after Ultrafast Excitation. *Nano Lett.* **2017**, *17*, 644–651.

(50) Chi, Z.; Chen, H.; Chen, Z.; Zhao, Q.; Chen, H.; Weng, Y. X. Ultrafast Energy Dissipation via Coupling with Internal and External Phonons in Two-Dimensional MoS_2. *ACS Nano* **2018**, *12*, 8961–8969.

(51) Chowdhury, R. K.; Nandy, S.; Bhattacharya, S.; Karmakar, M.; Bhaktha, S. N. B.; Datta, P. K.; Taraphder, A.; Ray, S. K. Ultrafast Time-Resolved Investigations of Excitons and Biexcitons at Room Temperature in Layered WS_2. *2D Mater.* **2019**, *6*, 015011.

(52) Poellmann, C.; Steinleitner, P.; Leierseder, U.; Nagler, P.; Plechinger, G.; Porer, M.; Bratschitsch, R.; Schüller, C.; Korn, T.; Huber, R. Resonant Internal Quantum Transitions and Femtosecond Radiative Decay of Excitons in Monolayer WSe_2. *Nat. Mater.* **2015**, *14*, 889–893.

(53) Hartland, G. V. Optical Studies of Dynamics in Noble Metal Nanostructures. *Chem. Rev.* **2011**, *111*, 3858–3887.

(54) Hartland, G. V. Ultrafast Studies of Single Semiconductor and Metal Nanostructures through Transient Absorption Microscopy. *Chem. Sci.* **2010**, *1*, 303–309.

(55) O'Brien, K.; Lanzillotti-Kimura, N. D.; Rho, J.; Suchowski, H.; Yin, X.; Zhang, X. Ultrafast Acousto-Plasmonic Control and Sensing in Complex Nanostructures. *Nat. Commun.* **2014**, *5*, 4042.

(56) Yi, C.; Dongare, P. D.; Su, M.; Wang, W.; Chakraborty, D.; Wen, F.; Chang, W.-S.; Sader, J. E.; Nordlander, P.; Halas, N. J.; *et al.* Vibrational Coupling in Plasmonic Molecules. *Proc. Natl. Acad. Sci.* **2017**, *114*, 11621–11626.

(57) Eizner, E.; Akulov, K.; Schwartz, T.; Ellenbogen, T. Temporal Dynamics of Localized Exciton-Polaritons in Composite Organic-Plasmonic Metasurfaces. *Nano Lett.* **2017**, *17*, 7675–7683.

(58) Zhao, W.; Wang, S.; Liu, B.; Verzhbitskiy, I.; Li, S.; Giustiniano, F.; Kozawa, D.; Loh, K. P.; Matsuda, K.; Okamoto, K.; *et al.* Exciton-Plasmon Coupling and Electromagnetically Induced Transparency in Monolayer Semiconductors Hybridized with Ag Nanoparticles. *Adv. Mater.* **2016**, *28*, 2709–2715.

(59) Lo, T. W.; Zhang, Q.; Qiu, M.; Guo, X.; Meng, Y.; Zhu, Y.; Xiao, J. J.; Jin, W.; Leung, C. W.; Lei, D. Thermal Redistribution of Exciton Population in Monolayer Transition Metal Dichalcogenides Probed with Plasmon-Exciton Coupling Spectroscopy. *ACS Photonics* **2019**, *6*, 411–421.

(60) Thomas, R.; Thomas, A.; Pullanchery, S.; Joseph, L.; Somasundaran, S. M.; Swathi, R. S.; Gray, S. K.; Thomas, K. G. Plexcitons: The Role of Oscillator

Strengths and Spectral Widths in Determining Strong Coupling. *ACS Nano* **2018**, *12*, 402–415.

(61) Zhang, Y.; Chen, W.; Fu, T.; Sun, J.; Zhang, D.; Li, Y.; Zhang, S.; Xu, H. Simultaneous Surface-Enhanced Resonant Raman and Fluorescence Spectroscopy of Monolayer $MoSe_2$: Determination of Ultrafast Decay Rates in Nanometer Dimension. *Nano Lett.* **2019**, acs.nanolett.9b02425.

(62) Yu, H.; Talukdar, D.; Xu, W.; Khurgin, J. B.; Xiong, Q. Charge-Induced Second-Harmonic Generation in Bilayer WSe_2. *Nano Lett.* **2015**, *15*, 5653–5657.

(63) Kang, Y.; Najmaei, S.; Liu, Z.; Bao, Y.; Wang, Y.; Zhu, X.; Halas, N. J.; Nordlander, P.; Ajayan, P. M.; Lou, J.; *et al.* Plasmonic Hot Electron Induced Structural Phase Transition in a MoS_2 Monolayer. *Adv. Mater.* **2014**, *26*, 6467–6471.

(64) Li, Z.; Ezhilarasu, G.; Chatzakis, I.; Dhall, R.; Chen, C. C.; Cronin, S. B. Indirect Band Gap Emission by Hot Electron Injection in Metal/MoS_2 and Metal/WSe_2 Heterojunctions. *Nano Lett.* **2015**, *15*, 3977–3982.

(65) Li, Y.; Distefano, J. G.; Murthy, A. A.; Cain, J. D.; Hanson, E. D.; Li, Q.; Castro, F. C.; Chen, X.; Dravid, V. P. Superior Plasmonic Photodetectors Based on Au@MoS_2 Core-Shell Heterostructures. *ACS Nano* **2017**, *11*, 10321–10329.

(66) Xu, X.; Luo, F.; Tang, W.; Hu, J.; Zeng, H.; Zhou, Y. Enriching Hot Electrons via NIR-Photon-Excited Plasmon in WS_2@Cu Hybrids for Full-Spectrum Solar Hydrogen Evolution. *Adv. Funct. Mater.* **2018**, *28*, 1804055.

(67) Johnson, P. B.; Christy, R. W. Optical Constants of the Noble Metals. *Phys. Rev. B* **1972**, *6*, 4370–4379.

(68) Li, Y.; Chernikov, A.; Zhang, X.; Rigosi, A.; Hill, H. M.; Van Der Zande, A. M.; Chenet, D. A.; Shih, E. M.; Hone, J.; Heinz, T. F. Measurement of the Optical Dielectric Function of Monolayer Transition-Metal Dichalcogenides: MoS_2, $MoSe_2$, WS_2, and WSe_2. *Phys. Rev. B* **2014**, *90*, 205422.